Silencing and enhancement of second-harmonic generation in optical gap antennas

Johann Berthelot,[1,2] **Guillaume Bachelier,**[3,4] **Mingxia Song,**[1] **Padmnabh Rai,**[1] **Gérard Colas des Francs,**[1] **Alain Dereux,**[1] **and Alexandre Bouhelier**[1,*]

[1] *Laboratoire Interdisciplinaire Carnot de Bourgogne CNRS-UMR 6303, Université de Bourgogne, 21078 Dijon, France*

[2] *Now at ICFO, The Institute of Photonic Sciences, Av. Carl Friedrich Gauss, 3, 08860 Castelldefels (Barcelona) Spain*

[3] *Laboratoire de Spectrométrie Ionique et Moléculaire, CNRS-UMR 5579, Université Claude Bernard Lyon 1, 69622 Villeurbanne, France*

[4] *Institut Néel, CNRS-UPR 2940, 38042 Grenoble cedex, France*

[*] *alexandre.bouhelier@u-bourgogne.fr*

Abstract: Amplifying local electromagnetic fields by engineering optical interactions between individual constituents of an optical antenna is considered fundamental for efficient nonlinear wavelength conversion in nanometer-scale devices. In contrast to this general statement we show that high field enhancement does not necessarily lead to an optimized nonlinear activity. In particular, we demonstrate that second-harmonic responses generated at strongly interacting optical gap antennas can be significantly suppressed. Numerical simulations are confirming silencing of second-harmonic in these coupled systems despite the existence of local field amplification. We then propose a simple approach to restore and amplify the second-harmonic signal by changing the manner in which electrically-connected optical antennas are interacting in the charge-transfer plasmon regime. Our observations provide critical design rules for realizing optimal structures that are essential for a broad variety of nonlinear surface-enhanced characterizations and for realizing the next generation of electrically-driven optical antennas.

OCIS codes: (180.4315) Nonlinear microscopy; (190.4720) Optical nonlinearities of condensed matter; (240.4350) Nonlinear optics at surfaces.

References and links

1. L. Novotny and N. F. Van Hulst, "Antennas for light," Nat. Photonics **5**, 83–90 (2011).
2. A. Bouhelier, M. Beversluis, A. Hartschuh, and L. Novotny, "Near-field second-harmonic generation induced by local field enhancement," Phys. Rev. Lett. **90**, 013903 (2003).
3. A. Bouhelier, R. Bachelot, G. Lerondel, S. Kostcheev, P. Royer, and G. P. Wiederrecht, "Surface plasmon characteristics of tunable photoluminescence in single gold nanorods," Phys. Rev. Lett. **95**, 267405 (2005).
4. J. Butet, J. Duboisset, G. Bachelier, I. Russier-Antoine, E. Benichou, C. Jonin, and P.-F. Brevet, "Optical second harmonic generation of single metallic nanoparticles embedded in a homogeneous medium," Nano Lett. **10**, 1717–1721 (2010).
5. M. Lippitz, M. A. van Dijk, and M. Orrit, "Third-harmonic generation from single gold nanoparticles," Nano Lett. **5**, 799–802 (2005).

#162701 - $15.00 USD Received 8 Feb 2012; revised 20 Mar 2012; accepted 1 Apr 2012; published 23 Apr 2012

6. M. Danckwerts, and L. Novotny, "Optical frequency mixing at coupled gold nanoparticles," Phys. Rev. Lett. **98**, 026104 (2007).
7. T. Hanke, G. Krauss, D. Träutlein, B. Wild, R. Bratschitsch, and A. Leitenstorfer, "Efficient nonlinear light emission of single gold optical antennas driven by few-cycle near-infrared pulses," Phys. Rev. Lett. **103**, 257404 (2009).
8. S. Kim, J. Jin, Y.-J. Kim, I.-Y. Park, Y. Kim, and S.-W. Kim, "High-harmonic generation by resonant plasmon field enhancement," Nature **453**, 757–760 (2008).
9. P. Mühlschlegel, H.-J. Eisler, O. J. F. Martin, B. Hecht, and D. W. Pohl, "Resonant optical antennas," Science **308**, 1607–1609 (2005).
10. H. Wang, T. B. Huff, D. A. Zweifel, W. He, P. S. Low, and A. W. J.-X. Cheng, "In vitro and in vivo two-photon luminescence imaging of single gold nanorods," Proc. Natl. Acad. Sci. USA **102**, 15752–15756 (2005).
11. N. J. Durr, T. Larson, D. K. Smith, B. A. Korgel, K. Sokolov, and A. Ben-Yakar, "Two-photon luminescence imaging of cancer cells using molecularly targeted gold nanorods," Nano Lett. **7**, 941–945 (2007).
12. A. García-Martín, D. R. Ward, D. Natelson, and J. C. Cuevas, "Field enhancement in subnanometer metallic gaps," Phys. Rev. B **83**, 193404 (2011).
13. J. Aizpurua, G. W. Bryant, J. Richter, F. J. García de Abajo, B. K. Kelley, and T.Mallouk, "Optical properties of coupled metallic nanorods for field-enhanced spectroscopy," Phys. Rev. B **71**, 235420 (2005).
14. A. Bouhelier, M. Beversluis, and L. Novotny, "Characterization of nanoplasmonic structures by locally excited photoluminescence," Appl. Phys. Lett. **82**, 5041–5043 (2003).
15. P. J. Schuck, D. P. Fromm, A. Sundaramurthy, G. S. Kino, and W. E. Moerner, "Improving the mismatch between light and nanoscale objects with gold bowtie nanoantennas," Phys. Rev. Lett. **94**, 017402 (2005).
16. P. Ghenuche, S. Cherukulappurath, T. H. Taminiau, N. F.van Hulst, and R. Quidant, "Spectroscopic mode mapping of resonant plasmon nanoantennas," Phys. Rev. Lett. **101**, 116805 (2008).
17. K. D. Ko, A. Kumar, K. H. Fung, R. Ambekar, G. L. Liu, N. X. Fang, J. Kimani, and C. Toussaint, "Nonlinear optical response from arrays of au bowtie nanoantennas," Nano Lett. **11**, 61–65 (2011).
18. B. Lamprecht, A. Leitner, and F. Aussenegg, "Shg studies of plasmon dephasing in nanoparticles," Appl. Phys. B **68**, 419–423 (1999).
19. B. Canfield, S. Kujala, K. Jefimovs, J. Turunen, and M. Kauranen, "Linear and nonlinear optical responses influenced by broken symmetry in an array of gold nanoparticles," Opt. Express **12**, 5418–5423 (2004).
20. M. D. McMahon, R. Lopez, R. F. Haglund Jr., E. A. Ray, and P. H. Bunton, "Second-harmonic generation from arrays of symmetric gold nanoparticles," Phys. Rev. B **73**, 041401 (2006).
21. C. Hubert, L. Billot, P.-M. Adam, R. Bachelot, P. Royer, J. Grand, D. Gindre, K. D. Dorkenoo, and A. Fort, "Role of surface plasmon in second harmonic generation from gold nanorods," Appl. Phys. Lett. **90**, 181105 (2007).
22. M. W. Klein, C. Enkrich, M. Wegener, and S. Linden, "Second-harmonic generation from magnetic metamaterials," Science **313**, 502–504 (2006).
23. M. D. McMahon, D. Ferrera, C. T. Bowie, R. Lopez, and R. F. Haglund Jr., "Second harmonic generation from resonantly excited arrays of gold nanoparticles," Appl. Phys. B **87**, 259–265 (2007).
24. Y. Zhang, N. K. Grady, C. Ayala-Orozco, and N. J. Halas, "Three-dimensional nanostructures as highly efficient generators of second harmonic light," Nano Lett. **11**, 5519–5523 (2011).
25. H. Husu, R. Siikanen, J. Mäkitalo, J. Lehtolahti, J. Laukkanen, M. Kuittinen, and M. Kauranen, "Metamaterials with tailored nonlinear optical response," Nano Lett. **12**, asap (2012).
26. J. I. Dadap, J. Shan, K. B. Eisenthal, and T. F. Heinz, "Second-harmonic rayleigh scattering from a sphere of centrosymmetric material," Phys. Rev. Lett. **83**, 4045–4048 (1999).
27. W. L. Mochán, J. A. Maytorena, B. S. Mendoza, and V. L. Brudny, "Second-harmonic generation in arrays of spherical particles," Phys. Rev. B **68**, 085318 (2003).
28. M. Finazzi, P. Biagioni, M. Celebrano, and L. Duò, "Selection rules for second-harmonic generation in nanoparticles," Phys. Rev. B **76**, 125414 (2007).
29. G. Bachelier, I. Russier-Antoine, E. Benichou, C. Jonin, and P.-F. Brevet, "Multipolar second-harmonic generation in noble metal nanoparticles," J. Opt. Soc. Am. B **25**, 955–960 (2008).
30. J. Butet, G. Bachelier, I. Russier-Antoine, C. Jonin, E. Benichou, and P.-F. Brevet, "Interference between selected dipoles and octupoles in the optical second-harmonic generation from spherical gold nanoparticles," Phys. Rev. Lett. **105**, 077401 (2010).
31. A. Bouhelier, R. Bachelot, J. Im, G. P. Wiederrecht, G. Lerondel, S. Kostcheev, and P. Royer, "Electromagnetic interactions in plasmonic nanoparticle arrays," J. Phys. Chem. B **109**, 3195–3198 (2005).
32. C. Huang, A. Bouhelier, G. Colas des Francs, A. Bruyant, A Guenot, E. Finot, J.-C. Weeber and A. Dereux, "Gain, detuning, and radiation patterns of nanoparticle optical antennas" Phys. Rev. B **78**, 155407 (2008).
33. W. Rechberger, A. Hohenau, A. Leitner, J. Krenn, B. Lamprecht, and F. Aussenegg, "Optical properties of two interacting gold nanoparticles," Opt. Comm. **220**, 137–141 (2003).
34. A. Slablab, L. Le Xuan, M. Zielinski, Y. de Wilde, V. Jacques, D. Chauvat, and J.-F. Roch, "Second-harmonic generation from coupled plasmon modes in a single dimer of gold nanospheres," Opt. Express **21**, 220–227 (2012).
35. G. Bachelier, J. Butet, I. Russier-Antoine, C. Jonin, E. Benichou, and P.-F. Brevet, "Origin of optical second-

#162701 - $15.00 USD Received 8 Feb 2012; revised 20 Mar 2012; accepted 1 Apr 2012; published 23 Apr 2012

harmonic generation in spherical gold nanoparticles: Local surface and nonlocal bulk contributions," Phys. Rev. B **82**, 235403 (2010).
36. B. K. Canfield, H. Husu, J. Laukkanen, B. Bai, M. Kuittinen, J. Turunen, and M. Kauranen, "Local field asymmetry drives second-harmonic generation in noncentrosymmetric nanodimers," Nano Lett. **7**, 1251–1255 (2007).
37. J.-S. Huang, J. Kern, P. Geisler, P. Weinmann, M. Kamp, A. Forchel, P. Biagioni, and B. Hecht., "Mode imaging and selection in strongly coupled nanoantennas," Nano Lett. **10**, 2105–2110 (2010).
38. S. Sheikholeslami, Y. W. Jun, P. K. Jai, and A. P. Alivisatos, "Coupling of optical resonances in a compositionally asymmetric plasmonic nanoparticle dimer," Nano Lett. **10**, 2655-2660 (2010).
39. Y. Pu, R. Grange, C.-L. Hsieh, and D. Psaltis, "Nonlinear optical properties of core-shell nanocavities for enhanced second-harmonic generation," Phys. Rev. Lett. **104**, 207402 (2010).
40. G. Volpe, S. Cherukulappurath, R. Juanola Parramon, G. Molina-Terriza, and R. Quidant, "Controlling the optical near field of nanoantennas with spatial phase-shaped beams " Nano. Lett. **9**, 3608–3611 (2009).
41. H. Park, A. K. L. Lim, J. Park, A. P. Alivisato, and P. L. McEuen, "Fabrication of metallic electrodes with nanometer separation by electromigration," Appl. Phys. Lett **75**, 301–303 (1999).
42. D. Ward, N. K. Grady, C. S. Levin, N. J. Halas, Y. Wu, P. Nordlander, and D. Natelson, "Electromigrated nanoscale gaps for surface-enhanced raman spectroscopy," Nano Lett. **7**, 1396–1400 (2007).
43. D. R. Ward, F. Hüser, F. Pauly, J. C. Cuevas, and D. Natelson, "Optical rectification and field enhancement in a plasmonic nanogap," Nature Tech. **5**, 732–736 (2010).
44. O. Pérez-González, N. Zabala, A. G. Borisov, N. J. Halas, P. Nordlander, and J. Aizpurua, "Optical spectroscopy of conductive junctions in plasmonic cavities," Nano Lett. **10**, 3090–3095 (2010).
45. A. Mangin, A. Anthore, M. L. Della Rocca, E. Boulat, and P. Lafarge, "Reduced work functions in gold electromigrated nanogaps," Phys. Rev. B **80**, 235432 (2009).
46. K. I. Bolotin, F. Kuemmeth, A. N. Pasupathy, and D. C. Ralph, "Metal-nanoparticle single-electron transistors fabricated using electromigration," Appl. Phys. Lett. **84**, 3154–3156 (2004).
47. S. Mahapatro, A. K. Ghosh, and D. Janes, "Nanometer scale electrode separation (nanogap) using electromigration at room temperature," IEEE Trans. Nanotech. **5**, 232–236 (2006).
48. B. Stahlmecke and G. Dumpich, "Resistance behaviour and morphological changes during electromigration in gold wires," J. Phys: Cond. Mat **19**, 046210 (2007).
49. K. Li, M. I. Stockman, and D. J. Bergman, "Enhanced second harmonic generation in a self-similar chain of metal nanospheres," Phys. Rev. B **72**, 153401 (2005).

1. Introduction

Metal optical nano-antennas are essential elements to enhance weak optical cross-sections and control light-matter interactions at the single emitter level [1]. Surface plasmon resonances, singular geometries, and electromagnetic coupling are physical mechanisms leading to large amplification factors. As a result, strong optical second [2–4], third [5–7] and higher-order nonlinearities [8,9] were observed at metal nanostructures forming thus the basis of surface-enhanced nonlinear imaging, spectroscopies and devices. These responses are particularly attractive as robust bio-compatible contrast agents in medical imaging [10, 11], but also as wavelength-conversion planar photonic components with resolutely reduced dimensions [8] mitigating thus the need for phase-matched processes required in bulk materials. In this context, optical gap antennas are largely exploited for their ability to drastically concentrate and amplify the electromagnetic field at the feed gap [12,13]. This was unambiguously demonstrated in coupled particle pairs where two-photon luminescence, four-wave mixing and third-harmonic generation were shown to increase until a conductive bridge was formed [6, 7, 14–17]. Second-harmonic generation (SHG) however, represents a peculiar nonlinear case since this process is forbidden within the dielectric dipole approximation in bulk centrosymmetric materials. Asymmetric particles are therefore typically required for producing an efficient harmonic response [18, 19] but are not strictly necessary [2, 20, 21]. An increase of the conversion yield was also observed for resonant excitation suggesting that large oscillator strengths and enhancement factors are instrumental for locally amplifying SHG [21–24].

In this communication, and in direct contradiction with other nonlinear responses, we show that SHG can be very efficiently suppressed in systems promoting high field amplification. Specifically, we demonstrate silencing of the SHG occurring at the gap of individual strongly-coupled optical antennas for a polarization condition promoting the largest coupling strength.

#162701 - $15.00 USD Received 8 Feb 2012; revised 20 Mar 2012; accepted 1 Apr 2012; published 23 Apr 2012

These results are confirmed by numerical simulations emphasizing the importance of nonlinear current symmetry in these systems. We propose a mechanism to restore the nonlinear response of an electrically-connected gap whereby SHG is efficiently amplified to create a localized source of radiating harmonic photons.

2. Results and discussion

Optical gap antennas constituted of Au nanorods were fabricated by standard electron-beam lithography and liftoff technique on a glass substrate. The dimensions of individual rods are 2.5 μm in length, 100 nm in width and 50 nm in height. The gap separation g is varied systematically from contact to 135 nm with a minimum separation of 15 nm. The antennas are separated by 2μm to avoid long-range coupling and grating-induced responses [23, 25]. Figure 1(a) displays scanning electron micrographs of optical gap antennas with g=0, 15 and 70 nm. The SHG response of individual antenna is spatially interrogated with a nonlinear confocal microscope. A 150 fs Titanium:Sapphire tuned at a fundamental wavelength of 810 nm is focused on the antennas in a diffraction-limited spot by a high numerical aperture objective (N.A.=1.49). The SHG is discriminated from the fundamental beam by combining a dichroic beam splitter and a narrow pass-band filter and is detected by an avalanche photodiode. The average intensity at the focal spot is kept constant at 310 MW/m^2. Figure 1(b) shows SHG maps for the optical gap antennas presented in Fig. 1(a). The polarization is adjusted along the main axis of the antennas.

For all investigated structures, the largest harmonic response is obtained at the uncoupled extremities (referred to as corners hereafter) while the SHG signal generated from the antenna body is barely above the background level. This is illustrated in the confocal map displayed in Fig. 1(b). SHG is usually promoted at interfaces where symmetry is broken. The corner response originates therefore from a rapid variation of the electric field across the interface [2, 26] under this heterogeneously focused illumination [27, 28]. Additional bulk contributions and field retardation effects can further contribute to the harmonic response [29, 30].

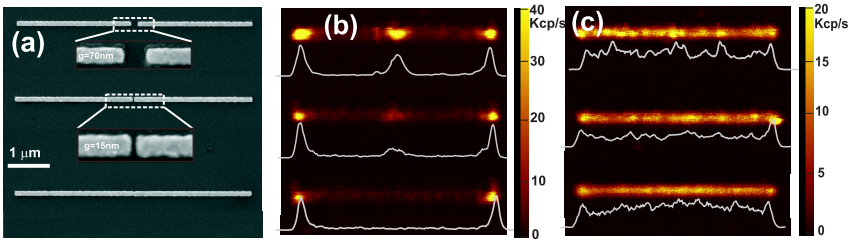

Fig. 1. (a) Scanning electron micrographs of three optical gap antennas with gap values g=0 (contact), 15 nm and 70 nm. Insets: magnified view of the gap area. (b) Second harmonic images of the corresponding antennas. The incident linear polarization is aligned with the long axis of the nanorods. (c) Corresponding SHG maps for a polarization perpendicular to the antenna axis. Intensity profiles along the wires are added on the bottom of each image. The image dynamics are limited to 40 Kcts/s and 20 Kcts/s in (b) and (c) respectively.

More interesting is the SHG response located in the gap area. For strongly coupled nanorods (g=15 nm), the SHG count rate at the gap is approximately one third of that detected at the corners as shown by the intensity profile in Fig. 1(b). For g=70 nm, corresponding to weakly coupled structures [31], the SHG count rate at the gap approaches that of the corners. We found that the SHG at the corners is almost constant for all investigated antennas ($\sim 40\pm5$ Kcts/s). This suggests that resonant higher-order modes of the antennas are not contributing to the sig-

#162701 - $15.00 USD Received 8 Feb 2012; revised 20 Mar 2012; accepted 1 Apr 2012; published 23 Apr 2012

nal. For an incident transverse polarization, the enhanced response at the corners is suppressed in favor of a SHG response distributed along the entire antenna length at around 15±5 Kcts/s as shown in Fig. 1(c). The SHG response at the gaps are barely distinguishable. SHG for this polarization is understood in terms of rapid variation of the electric field across the metal interface occurring along the entire antenna length. In contrast, the tangential component of the electric field is continuous at both rods extremities (corner and gap) and does not lead to an efficient SHG generation. The SHG count rate along the rods for a perpendicular polarization is systematically weaker than the corner response for a cross-polarization, mitigating thus the existence of a strong resonant contribution. The longitudinal dipolar resonance for these antennas is above 3.5 μm [13] implying that the antennas are not driven resonantly at 810 nm. The advantage at working off-resonance is that the only variable in the present investigation is the gap size. The antennas are therefore wavelength-insensitive and data interpretation is drastically simplified. We confirmed the non-resonant character of the antennas by imaging their Rayleigh scattering at a wavelength of 810 nm corresponding to the fundamental wavelength and at the 457 nm krypton line mimicking the second harmonic wavelength (405 nm). Any resonant excitation of a particular antenna would provide an increased Rayleigh scattering response [32]. Figure 2 shows confocal maps of the optical gap antennas for the two considered wavelengths and for two orthogonal polarizations. The scattered intensity remains constant between individual antenna pairs (variation $<$5%) indicating that a resonant excitation at the fundamental and near-to-harmonic wavelengths is unlikely.

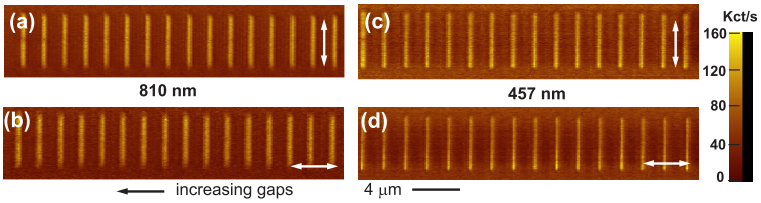

Fig. 2. (a) and (b) Backscattered confocal Rayleigh maps of a series of antennas separated by increasing gaps at the fundamental wavelength (810 nm) for two polarization orientations, respectively (arrows). (c) and (d) Scattered maps of the same series at an excitation wavelength of 457 nm close to the harmonic response and for the two relevant polarizations, respectively. The scattered intensity is constant between antennas indicating a non-resonant excitation. The first four antennas on the right hand side of the imaged are bridged. The last antenna on the left has a gap of 135 nm, barely resolved in the images.

In order to quantify the nonlinear efficiency of the antenna gap, a normalized SHG signal $\Gamma = I_g/I_c$ is introduced, where I_g and I_c correspond to the measured count rates integrated in 880 nm$\times$440 nm areas located over the gap and the corners, respectively. I_c is a value representing the signal averaged at the two uncoupled extremities. We found that Γ strongly depends on the gap distance g. The results obtained for 24 antennas are shown in Fig. 3(a) for longitudinal and transverse incident polarizations, respectively. For longitudinal excitation, Γ is below unity for strongly-coupled antennas and increases with the gap size. Since $\Gamma < 2$, we conclude that the facing corners constituting the gap are not entirely decoupled for the gap range considered here.

As shown in Fig. 3(a), the averaged Γ value is around unity for transverse incident polarization. The dispersion in the data points is attributed to minor geometrical differences inherent to the fabrication method. Small inhomogeneities of the SHG intensity recorded at the location of the gap are visible on the cross sections displayed in Fig. 1(c) and are thus influencing the normalized parameter Γ. Unlike for longitudinal excitation, no specific trend is observed

#162701 - $15.00 USD Received 8 Feb 2012; revised 20 Mar 2012; accepted 1 Apr 2012; published 23 Apr 2012

while scaling down the gap size. The complete polarization dependence of Γ is displayed in Fig. 3(b) for a 36 nm-gap and shows a monotonous evolution: the SHG response at the gap evolves between 0.5 and 1.5 times that of the uncoupled extremities, for a longitudinal and transverse polarization, respectively. Note that for a transverse polarization, the antenna remains wavelength-insensitive since the blue-shift of the resonance with decreasing gap size is typically of few nanometers [33].

The results of Fig. 3(a) demonstrate that SHG is significantly silenced for strongly coupled antennas. This behavior contradicts what is commonly observed for other types of nonlinear signals such as two-photon luminescence [16] and third harmonic generation (THG) [7] whereby strong coupling is at the origin of enhanced responses at the gap. The evolution of Γ with the gap size [Fig. 3(a)] confirms the SHG observation of Slablab and co-workers for resonant particle dimers but contradicts their interpretation [34]. These authors concluded that the strong SHG signal arising for nearly touching particles is due to a large resonant enhancement of the fundamental electric field at the location of the gap. We show in the following that the symmetry of the harmonic field significantly differs from the fundamental one and leads to a cancelation of the harmonic photons for self-similar dimers.

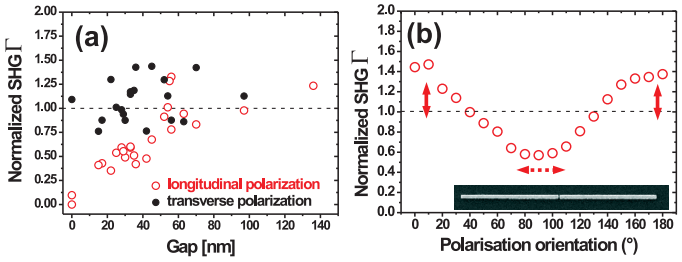

Fig. 3. (a) Evolution of the normalized SHG value Γ as a function of gap distance for two different polarization orientations. (b) Polarization dependance of Γ for an optical gap antenna with g=36 nm.

Numerical simulations are conducted based on finite element method [29, 35]. Briefly, the fundamental electric field $\mathbf{E}(\mathbf{r},\omega)$ is computed using the scattered field formulation with a plane wave excitation, and is used to evaluate the nonlinear currents in a first step. In the present case, the simulations are restricted to the normal surface current $j_{s,\perp}(\mathbf{r},2\omega)$:

$$j_{s,\perp}(\mathbf{r},2\omega) = \frac{\partial P_{s,\perp}(\mathbf{r},2\omega)}{\partial t} = -2i\omega\chi_{s,\perp\perp\perp}E_{\perp}^{2}(\mathbf{r},\omega) \tag{1}$$

where $\perp$ stems for the component normal to the particle surface, $\chi_{s,\perp\perp\perp}$ is the nonlinear surface susceptibility and $P_{s,\perp}$ is the corresponding surface polarization oscillating at the frequency 2ω just above the particle surface. $E_{\perp}$ is evaluated inside the particle. The normal surface current current acts as a nonlinear source for the harmonic field which can be determined in a second step by solving Maxwell's equations in the near-field region [29]. The SHG scattering cross section $C_{\mathrm{scat}}^{2\omega}$ is shown in Fig. 4(a) for Au nanorods with a radius R =15 nm and an aspect ratio of 3.1. Simulating nanorods with sizes closer to the experimental ones is not possible due to the available computer memory.

Due to a field enhancement effect, SHG from a single nanorod is strongly amplify when the fundamental wavelength matches the surface plasmon resonance [21], which is around 800 nm for the considered rod. As expected from two interacting nanoparticles, the maximum of second-harmonic scattering cross section is shifted toward a longer fundamental wavelength

#162701 - $15.00 USD Received 8 Feb 2012; revised 20 Mar 2012; accepted 1 Apr 2012; published 23 Apr 2012

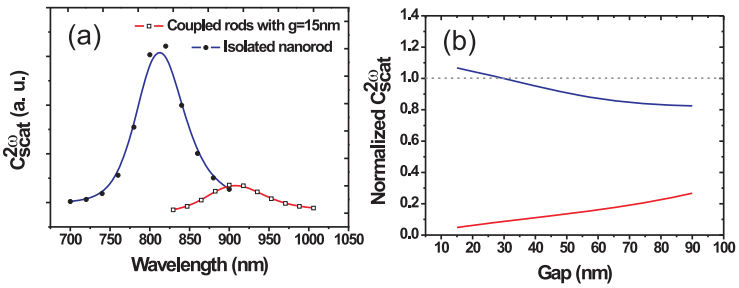

Fig. 4. (a) SHG scattering cross-sections as a function of the fundamental wavelength for an isolated rod (blue curve with plain dots) and for two aligned rods separated by g=15 nm (red curve with open squares). The fundamental electric field is parallel to the rod axis. The dimension of the rods are radius R=15 nm and aspect ratio of 3.1. (b) Evolution of the SHG scattering cross sections for an off-resonant excitation at 700 nm normalized to that of two isolated rods as a function of the radius R and for both longitudinal and transverse polarizations.

(∼900 nm) for antennas coupled by a gap g= 15 nm. Surprisingly, this shift is associated with a clear decrease of $C^{2\omega}_{\text{scat}}$. Such reduction of the SHG scattering efficiency is in clear contrast with the amplification mechanism commonly expected from hot-spots in paired antennas. In order to check whether the calculated SHG reduction is particular to a resonant fundamental excitation, we investigated the off-resonant nonlinear response of the coupled rods for both longitudinal and transverse excitations. The results are presented in Fig. 4(b) as a function of the gap g for a fundamental 700 nm off-resonance wavelength. For the smallest gap (g=R=15 nm), a clear reduction of $C^{2\omega}_{\text{scat}}$ from , in qualitative agreement with the experimental data. However, one might argue in this case that the isolated rods are excited closer to the resonance than the dimer favoring a higher intensity for the isolated rods (see Fig. 4(a)). But increasing the gap up to 90 nm (corresponding approximately to the rod length), $C^{2\omega}_{\text{scat}}$ is still largely smaller than for isolated rods, even if for such large gaps the rods are usually considered as weakly coupled. This analysis indicates that the partial SHG suppression is an intrinsic property of the gap and does not depend on the resonant character of the excitation.

In contrast, the SHG scattering cross section for a transverse excitation is close to unity for small gaps ($g \sim R$), here again in qualitative agreement with the experimental observations. The excitation being off-resonant regardless of the gap, one can conclude that the gap has only a weak effect for this polarization configuration. However and interestingly, the calculated scattered intensity decreases below that of uncoupled rods for larger gap sizes. This indicates that long range coupling (at the wavelength scale) take place between the two rods. This result contrasts with the experimental data and is a direct consequence of the specific configuration used for the simulation dealing with small rods excited by a plane wave.

To understand the silencing of SHG gap response, we plot in Fig. 5(a)-5(d) the spatial distribution of the electric field amplitudes calculated at the fundamental and harmonic wavelengths for two different gaps. The optical gap antennas (R =15 nm and an aspect ratio of 3.1) are excited off resonance at a wavelength of 700 nm. For longitudinal polarization, the near-field amplitudes at both frequencies are enhanced for the smallest gap, clearly forming a region of high electric field located in the interstice. This is expected from the nonlinear current expression (Eq. (1)) due to field enhancement but in apparent contradiction with the evolution of the calculated $C^{2\omega}_{\text{scat}}$ (Fig. 4(b)). Considering Eq. (1), one can easily show that for a longitudinal excitation, the nonlinear currents at the apex of an isolated rod have opposite directions. As a consequence of the centrosymmetry of the isolated nanoparticle, the far field contribution

#162701 - $15.00 USD Received 8 Feb 2012; revised 20 Mar 2012; accepted 1 Apr 2012; published 23 Apr 2012

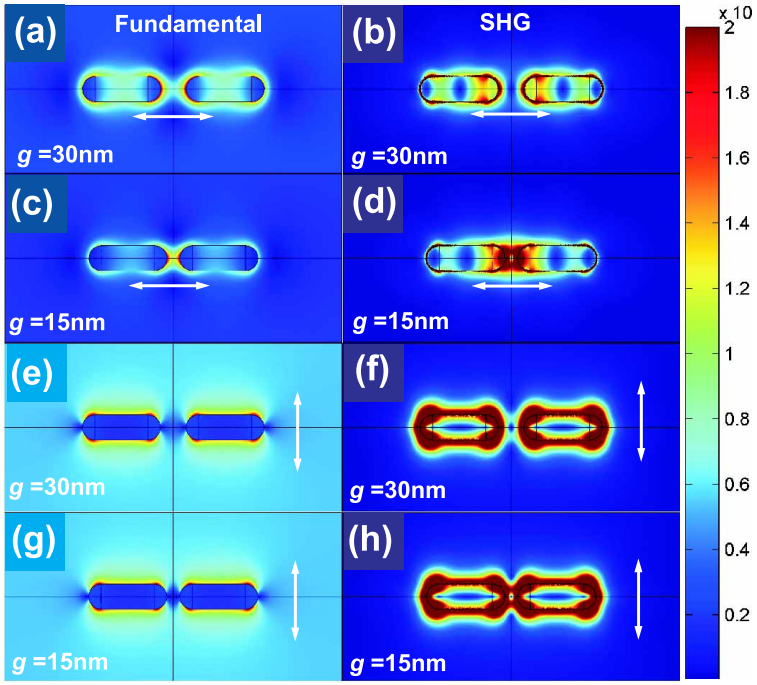

Fig. 5. Near field images of the fundamental (left column) and harmonic (right column) electric field amplitude around the optical gap antenna. gap sizes and polarizations are indicated on the maps. The presence of a minimum in the second harmonic amplitudes at the feed gap in (b) and (d) is characteristic of a nonradiative harmonic field distribution.

of the currents cancels out in the dipolar approximation, indicating that SHG is not an efficient process in noble metal nanostructures [4]. Coupling particles along their long axes retains the centrosymmetry of the system, preserving thus the nonradiative nature of the SHG antenna mode. The nonradiative character of the harmonic response is clearly seen as a vanishing amplitude at the gap center in Fig. 5(b) and 5(d) which is not observed at the fundamental frequency (Fig. 5(a) and 5(c)). This is perhaps better observed in Fig. 6 (a) and 6(b) where the real part the electric field along the polarization is represented. While the field at the gap is oscillating in phase at the fundamental wavelength, the coupled corners are clearly out of phase at the harmonic wavelength. While smaller gaps are associated to larger nonlinear currents, their contribution to the far-field is reduced as the result of their opposite oscillating directions. In other words, despite a near-field enhancement, the net result is a decrease of the far-field SHG while decreasing the gap size, in agreement with our experimental results.

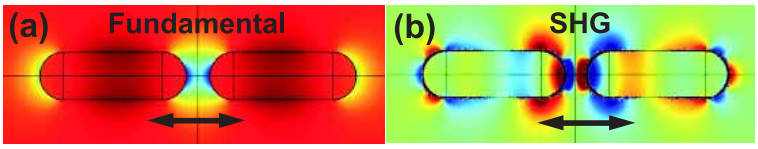

Fig. 6. (a) and (b) Calculated near-field maps of the real part of the longitudinal electric field at the fundamental and harmonic wavelengths, respectively. *g* is 15 nm. The fields at the coupled corners are oscillating out of phase at the harmonic wavelength indicating the nonradiative nature of the mode.

#162701 - $15.00 USD Received 8 Feb 2012; revised 20 Mar 2012; accepted 1 Apr 2012; published 23 Apr 2012

The same argumentation holds for a resonant excitation, explaining thus why the largest $C_{\mathrm{scat}}^{2\omega}$ is reduced in Fig. 4(a) for coupled antennas compared to isolated rods. For an optical gap antenna resonating at the fundamental wavelength, the SHG response of the gap would certainly be amplified compared to an off-resonant structure. However, the effect of the gap on the harmonic signal is convoluted with the wavelength sensitivity of the structure, hiding thus the importance of harmonic field symmetry. This conclusion may help to understand the observation of Slablab and co-workers where the fundamental excitation wavelength was in resonance with the investigated dimer [34].

For transverse excitation, neither the linear nor the harmonic properties are strongly affected by the gap size (see Fig. 5(e) and 5(h)), confirming the experimental results of Fig. 3(a). The strong gap dependence of the SHG signal for longitudinal excitation is specific to the symmetry of the dimers investigated here: for T-shaped arrangement, the nonlinear response leads to an increase of the SHG efficiency while scaling down the gap size [36].

Since enhancing SHG signal arising at noble metal nanostructures is a challenge for designing practical applications, the possibility to break the symmetry of the nonradiative harmonic mode is investigated in the following. Heterodimers, core-shell particles and high-order beams were successfully employed for changing the nature of an anti-bonding nonradiative mode [36–40]. Our approach is different and relies on the intrinsic geometry of a truly nanometer gap fabricated by electromigrating (EM) Au nanowires [41]. EM tunneling gaps are widely used in molecular electronics and were recently investigated for their large enhancement response [42], rectifying characteristics [43] and are promising candidates to study charge-transfer plasmons [44].

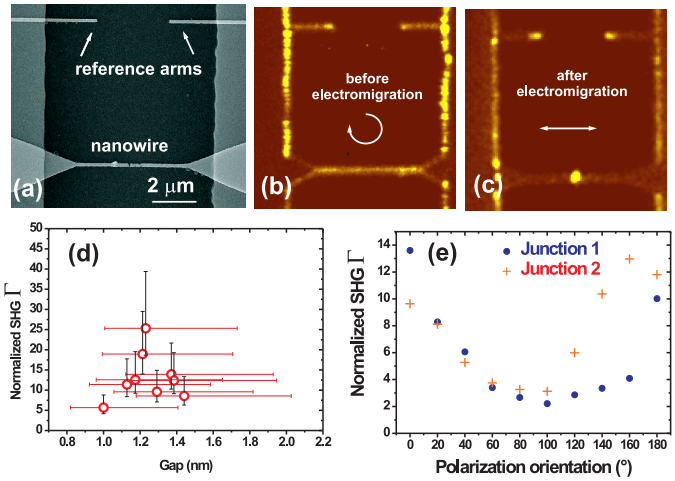

Fig. 7. (a) Scanning electron micrograph of a typical electromigrated nanowire and the two uncoupled reference arms. (b) and (c) Confocal SHG maps of the area before and after electromigration, respectively. A strong nonlinear signal is observed at the location of the tunnel junction. The arrows indicate the polarization state. (d) Evolution of Γ for a series of electromigrated junctions as a function of inferred nanometer gaps. (e) Polarization sensitivity of Γ for two electromigrated junctions. The SHG signal at the junction is enhanced for all measured gaps and polarization orientations.

Au nanowires [5 μm (length) × 100 nm (width) × 50 nm (height)] are fabricated by electron beam lithography and are electrically connected by a taper geometry to a set of macroscopic gold electrodes fabricated by UV-lithography. Figure 7(a) shows a typical micrograph of a Au nanowire lithographed on a glass substrate after EM process. The two upper arms are used

#162701 - $15.00 USD Received 8 Feb 2012; revised 20 Mar 2012; accepted 1 Apr 2012; published 23 Apr 2012

as references for estimating Γ. The SHG maps of the corresponding area before EM are presented in Fig. 7(b) for circular polarization to facilitate sample recognition. The reference arms and the nanowire are easily recognized in this SHG image. Because UV lithography renders rougher edges, the SHG signal is typically larger than the signal measured from edges defined by electron-beam lithography. Figure 7(c) shows the SHG map of the same area after EM of the nanowire for a polarization aligned with the nanowire. In this case, a strong SHG response is observed at the location of the junction: the SHG exceeds by a factor 17 that of the reference arms, a value in direct contradiction with the gaps fabricated by electron-beam lithography (Fig. 3(a)).

We have plotted in Fig. 7(d) the value of Γ for a series of tunnel junctions with gap size g ranging from 1 nm to 1.4 nm. g was deduced from differential conductance measurements using protocols outlined in Ref. [43, 45]. Electron tunneling with typical nonlinear transfert characteristics is observed under ambient condition for about 20% of the EM junctions. Figure 7(d) shows that the SHG signal is systematically amplified for EM gaps. For the considered range, we did not observe an obvious dependance of Γ with gap size. Instead, the magnitude of Γ is fairly dispersed from a junction to another. The relative large error bars on the determination of the gaps are the consequence of the uncertainty of the work function ϕ. For the tunnel junctions measured in this study we found an average value of $\tilde{\phi}$=0.8 $\pm$ 0.3 eV. This value is significantly lower than the bulk value ($\sim$ 5.4 eV). In a recent study, A. Mangin *et al.* [45] also reported reduced work functions in similar systems. This was explained by a contamination of the electrodes operating at ambient atmosphere and a drastic effect of the image potentiel. We have also evaluated Γ for electromigrated gaps where g could not be inferred from differential conductance measurement (non-tunneling regime) and measured slightly smaller Γ ($1 < \Gamma < 9$).

We hypothesize that the difference between the SHG response of lithographed gaps and electromigrated junctions originates from the geometry of the gap itself. While the interstices of Fig. 1 are rather well defined with plane-parallel coupled extremities, electromigrated polycrystalline Au nanowires are notoriously known to have meandered gaps [42, 46–48]. As illustrated in Fig. 8 (a) and 8(b), while the centrosymmetry of the lithographed gap is preserved, the typical geometry of an electromigrated gap is ill-defined, and like self-similar chains possesses no center of symmetry [49] promoting thus a large nonlinear response. It is important to note that even with asymmetric dimers *e.g.* T-shaped structures as in [36], the gaps are usually formed by plane-parallel facets. Our approach however, enables a complex structuring of the gap itself mitigating thus the effect of SHG symmetry in nanoscopic feed-gap regions.

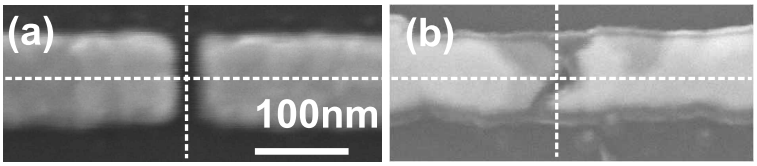

Fig. 8. High-resolution scanning electron micrographs picturing the intrinsic geometrical differences between a gap fabricated by electron-beam lithography (a) and a gap resulting from an electromigration process (b).

3. Conclusions

In summary, we have shown both experimentally and theoretically that the far-field second-harmonic response of optical gap antennas can be significantly silenced, where other types of nonlinear signals are usually strongly amplified. In contrast, the near-field efficiency follows the expected trend underlying the symmetry induced-origin of the far-field signal suppression.

#162701 - $15.00 USD Received 8 Feb 2012; revised 20 Mar 2012; accepted 1 Apr 2012; published 23 Apr 2012

By investigating off-resonant gap antennas, we have discriminated the role of symmetry usually hidden in wavelength-dependent responses. We further demonstrate that second-harmonic response can be restored and amplified by structuring the gap morphology using electrically connected nanometer-size electromigrated tunnel junctions. These results provide elements for designing optimal frequency-conversion optical antennas and will impact research employing surface-enhanced nonlinear spectroscopies as a prime characterization tool. Second-harmonic imaging enables a unique contrast mechanism to characterize the symmetry and surface quality of electromigrated tunnel junctions widely used in molecular electronics. Finally, optical gap antennas operating in the tunneling regime enables a self-aligned spatial overlap between region of high static electric field strength and area generating enhanced optical responses. This unique configuration can be exploited for realizing electron-fed optical antennas.

Acknowledgments

This work was funded by NanoSci E+ program under grant E^2-PLAS (ANR-08-NSCI-007) and the regional council of Burgundy program PARI Nanophotonique et Nanofabrication. A. B. acknowledges vivid discussions with H. Giessen from Stuttgart University and L. Le Xuan from Ecole Normale Supérieure de Cachan.

#162701 - $15.00 USD Received 8 Feb 2012; revised 20 Mar 2012; accepted 1 Apr 2012; published 23 Apr 2012